Monte Carlo-Based Modeling of Secondary Particle Tracks Generated by Intermediate- and Low-Energy Protons in Water

Alexey Verkhovtsev, Pedro Arce, Antonio Muñoz, Francisco Blanco and Gustavo García

Abstract This chapter gives an overview of recent developments in the Monte Carlo-based modeling of the interaction of ionizing radiation with biologically relevant systems. Several track structure codes, such as Geant4 (GEometry ANd Tracking 4), Geant4-DNA, and LEPTS (Low-Energy Particle Track Simulation), are described. Main features, areas of application and current limitations of each tool are discussed. A special attention is focused on the energy range covered by primary and secondary charged particles and on the type of interactions included in the simulation. A recent development of LEPTS is presented, aimed at the simulation of full slowing-down of protons in water together with all molecular processes involving secondary particles. The utilized approach allows one to study radiation effects on the nanoscale in terms of the number and the type of induced molecular processes.

A. Verkhovtsev (✉) · G. García
Instituto de Física Fundamental, Consejo Superior de Investigaciones Científicas (CSIC), Serrano 113-bis, 28006 Madrid, Spain
e-mail: verkhovtsev@iff.csic.es

G. García
e-mail: g.garcia@iff.csic.es

A. Verkhovtsev
MBN Research Center, 60438 Frankfurt am Main, Germany

P. Arce
Medical Applications Unit, Centro de Investigaciones Energéticas, Medioambientales y Tecnológicas (CIEMAT), Av. Complutense 40, 28040 Madrid, Spain
e-mail: pedro.arce@ciemat.es

A. Muñoz
Scientific Computing Unit, Centro de Investigaciones Energéticas, Medioambientales y Tecnológicas (CIEMAT), Av. Complutense 40, 28040 Madrid, Spain
e-mail: roldan@ciemat.es

F. Blanco
Departamento de Física Atómica, Molecular y Nuclear, Universidad Complutense de Madrid, Plaza de Ciencias 1, 28040 Madrid, Spain
e-mail: pacobr@fis.ucm.es

G. García
Centre for Medical Radiation Physics, University of Wollongong, Wollongong, NSW 2522, Australia

A.V. Solov'yov (ed.), *Nanoscale Insights into Ion-Beam Cancer Therapy*,
DOI 10.1007/978-3-319-43030-0_3

Development of new tools for the simulation of biologically relevant materials opens the way for a more realistic, physically meaningful description of radiation damage in living tissue.

1 Introduction

Understanding radiation effects produced by charged projectiles traversing biological media is of great interest in radiation biology, radiation therapy, and environmental radiation protection. An important feature of the interaction of ionizing radiation with biological systems is the complexity of produced damage [1]. It is well-established nowadays that the great portion of biodamage resulting from ionizing radiation is related to secondary electrons, free radicals and other reactive species, which are produced by ionizing and exciting molecules of the medium [1–3]. All these secondary species have been found to be more efficient in producing damage than the primary radiation, because they can effectively trigger physicochemical processes leading to molecular structure alterations, for instance, to covalent bond breaking, ionization, or negative ion formation [4]. In this context, "event-by-event" Monte Carlo simulation codes [5–11] as well as the phenomenological multiscale approach to the assessment of radiation damage [3] have been developed in order to model the effects of radiation on the nanoscale and to explore their correlation with the observed damage.

The discovery of radiation damage in biomolecular systems by low-energy electrons [2, 12, 13] has led to the development of the concept of nanodosimetry. It aims at a detailed description of the interaction processes occurring in nanometer-size volumes of the medium and of implications of these processes in terms of radiation damage, such as the number of ionization or dissociative events, type of generated secondary species, etc. A thorough understanding of the mechanisms of biodamage done by ionizing radiation requires evaluation of molecular-level effects related to dose deposition on the nanoscale [5, 14]. For that purpose, deep knowledge of numerous interactions induced by charged particles traversing living matter is strongly essential. A comprehensive description of the mechanisms underlying these interactions may ultimately lead to the development of new strategies and protocols in modern treatment techniques with ionizing radiation [15].

One of the widely used methods to study these effects in detail is based on Monte Carlo simulations performed by the track structure codes [5–11]. By sampling a sufficiently large number of tracks and averaging over the ensemble obtained, Monte Carlo simulations can provide valuable information about the mechanisms of the interaction of radiation with matter [1].

A Monte Carlo approach aims at the detailed simulation of trajectories of single particles in a medium, i.e. the complete track structure of the projectile and all secondary particles generated in the medium [16]. Thus, a good quantification of interaction parameters in a broad energy range is required. A common way to precisely determine the physical and chemical events occurring on the nanoscale is to

utilize models that can describe energy-loss processes in the medium in terms of interaction cross sections. Improving the accuracy of these models requires a considerable amount of interaction data that must be obtained from experiments and theoretical approaches. For modeling radiation damage in biological media, establishing an accurate and complete set of cross sections is thus of crucial importance. Being the primary input for track structure codes, such data should include appropriate integral and differential cross sections, energy loss spectra, and scattering cross sections for all kinds of inelastic events, in particular for those leading to molecular dissociations, chemical alterations and radical formation.

In recent years, substantial experimental and theoretical progress has been made to provide the essential data that describe how low-energy electrons, which are responsible for a significant non-repairable damage in biological systems, interact with the key molecular building blocks of living tissue, such as water and structural components of DNA and RNA molecules [17]. By means of the Low-Energy Particle Track Simulation (LEPTS) code (see the review paper [5] and references therein), it has become possible to model dynamics of secondary species down to the (sub-)electronvolt scale. This Monte Carlo-based tool has been developed to address the molecular level mechanisms of biodamage and to describe radiation effects in nanovolumes in terms of induced molecular dissociations [6]. LEPTS is based on reliable and self-consistent databases of interaction cross sections and energy-loss distributions compiled from experimental data and complemented with theoretical calculations. Up to now, these databases have been available for electrons and positrons [5].

The LEPTS methodology has been recently integrated [16] into the Geant4 (GEometry ANd Tracking 4) Monte Carlo toolkit [18, 19] as a new physics model for the simulation of low-energy electrons and positrons in relevant biological systems. As a result, it has become possible to select different sets of models for different energy intervals of the traced particles, for instance, using standard electromagnetic models, such as Livermore or Penelope, for high energies and LEPTS for low energies [16].

This chapter reports on the recent developments in the Monte Carlo-based modeling of the interaction of ionizing radiation with biologically relevant systems. We describe several widely utilized Monte Carlo track structure codes, such as Geant4 and Geant4-DNA [10]—an extension of Geant4 allowing for microdosimetric studies of biological damage induced by ionizing radiation. We also present an extension of the LEPTS methodology aiming at the explicit simulation of the slowing-down of heavy charged particles propagating through a biological medium, accounting for the production of secondary particles, including low-energy electrons, and a variety of induced molecular processes. Main features, areas of application and current limitations of each simulation tool are discussed. A special attention is paid to the energy range covered by primary and secondary charged particles and on the type of interactions included in the simulation.

As a case study, we present the results of the simulation of intermediate- and low-energy protons (starting from 1 MeV until their final thermalization down to the few-eV scale) traversing liquid water that is the main constituent of living tissue. Charged heavy particles of such energies contribute greatly to the maximum of energy

deposition in the Bragg peak region [20]. The utilized approach allows one to study radiation effects on the nanoscale in terms of the number and the type of induced molecular processes. The analysis performed thus provides valuable information which may be used further to improve modern treatment techniques based on proton- or heavy ion therapy.

In the following sections, we briefly describe the main capabilities of the Geant4, Geant4-DNA and LEPTS packages. Then, we present the recent development of LEPTS aimed at the simulation of full slowing-down of protons in water. In order to include protons into the simulations, a comprehensive dataset of integral and differential cross sections of elastic and inelastic scattering of intermediate- and low-energy protons from water molecules has been compiled; this dataset is also described.

2 The Geant4 Monte Carlo Simulation Tooklit

The Geant4 toolkit [18, 19] provides a versatile and comprehensive software package for simulating the passage of particles through matter. It includes a complete range of functionality including geometry, tracking of particles through materials and external electromagnetic fields, physics models, and the visualization of geometry and particle trajectories. To manage particle interactions, a set of complementary or alternative physics models are offered, covering a comprehensive range of physics processes which include electromagnetic, hadronic and optical ones, over a wide energy range starting, in some cases, from eV energies and being extended up to the TeV energy range in other cases. To build these physics models, data and expertise have been drawn from many sources around the world and in this respect, Geant4 acts as a repository that incorporates a large part of all that is known about particle interactions. Moreover, it continues to be refined, expanded and developed.

The toolkit is the result of a worldwide collaboration of physicists and software engineers. It has been created exploiting software engineering and object-oriented technology and implemented in the C++ programming language. While its first release in 1998 was designed for High Energy Physics, thanks to its big flexibility, the utilities needed for other fields, like Nuclear Physics, Space Physics, and Medical Physics, were also added soon after. Concerning Medical Physics, several projects were also developed in the fields of radiation therapy (external beams and brachytherapy), hadron therapy, positron emission tomography, and later on, in microdosimetry and radiobiology.

In the field of proton therapy, it is still common to use for treatment planning commercial software based on analytical methods that employ different physics approximations. Nevertheless, Monte Carlo-based treatment planning systems are slowly entering the market being recognized as a precise tool for this type of calculations [21–29].

2.1 Geant4 Physics for Proton Therapy Simulation

The detailed simulation of a proton therapy treatment requires the selection of the appropriate physics models, including the electromagnetic interactions of protons and other particles [30]. Geant4 offers several models to handle the electromagnetic interactions of leptons, photons, hadrons, and ions. In most of these models, the interactions of charged particles are treated in a condensed approach to avoid excessive CPU time. This means that many ionization and bremsstrahlung interactions are not simulated but these interactions may result in the emission of secondary particles with the energy above a threshold, which is set by the user. The energy of the non-simulated interactions is then summed up and treated as a local energy deposit. In a similar way the elastic scattering of charged particles is treated in a "multiple scattering" approach, condensing all the interactions of a particle in the calculation of the global deviation in position and direction. Among the three main categories of models available to treat electromagnetic interactions of charged particles and energetic photons, i.e. standard, Livermore and Penelope, the standard model is the preferred one for proton therapy simulation [22–24] as it offers enough precision while keeping an optimized CPU time consumption. In the case of multiple scattering, the preferred model is the Urban model, which uses functions to determine the angular and spatial distributions after a step chosen in such a way as to give the same moments of the (angular and spatial) distributions as are given by the Lewis theory [31].

Concerning hadronic physics, Geant4 provides a vast number of possible models, so that the user is able to choose those best matching the particle types, energy ranges, and other characteristics particular to a given simulation. In the case of proton therapy, there is a vast literature discussing the most appropriate models, but it seems that the binary cascade model is the preferred choice [32–34]. The Geant4 binary cascade model is an intra-nuclear cascade model in which an incident hadron collides with a nucleon, forming two final-state particles, one or both of which may be resonances. The resonances then decay hadronically and the decay products are propagated through the nuclear potential along curved trajectories until they re-interact or leave the nucleus. The remaining fragment is treated by precompound and de-excitation models.

2.2 The Geant4 DNA Physics Package

As mentioned above, the electromagnetic physics in Geant4 treats the charged-particle interaction in a condensed way and does not allow one to simulate the interactions of low-energy electrons. Subsequently, it is not possible to assess with these models the biological damage induced by ionizing radiation at the cellular (micrometer and below) scale. To fill this gap, a preliminary set of physics processes adapted to microdosimetry in liquid water down to the electronvolt scale was deliv-

ered into the Geant4 toolkit in 2007 [35] and has been improved since then [10, 36–41]. The package named Geant4-DNA has been developed to introduce specific functionalities in Geant4, allowing for:

(i) The modeling of elementary physical interactions between ionizing particles of energies down to the electronvolt scale in biological media (liquid water and DNA), during the so-called "physical" stage.
(ii) The modeling of the "physico-chemical and chemical" stages corresponding to the production and diffusion of oxidative radical species, and the chemical reactions occurring between them. During the "physico-chemical" stage, the water molecules that were excited and ionized during the physics stage may de-excite and dissociate into molecular radical species. In the "chemical" stage, these radicals diffuse in the medium surrounding the DNA. They may eventually react among themselves or with the DNA molecule. Studies using radical scavengers have demonstrated that at low values of linear energy transfer (LET), these radical species are responsible for most of the damages caused to the DNA molecule, showing a selective behavior in the type and localization of the damage, and also play a significant contribution at high values of LET.
(iii) The modeling of a "geometrical" stage where the two above stages are combined with a geometrical description of biological targets, such as chromatin segments or the cell nucleus. In particular, it is possible to implement the geometry of biological targets with a high resolution at the sub-micron scale and to track particles within these geometries using the Geant4-DNA physics processes.

At present, the Geant4-DNA extension set covers the dominant interactions of light particles and ions, including electrons, protons, hydrogen atoms, neutral and charged helium atoms, down to the eV scale in liquid water which is the main component of biological matter. The physics models and their experimental validation are described and discussed in detail in Refs. [26–34]. Some of these models are purely analytical, others make use of interpolated cross section data tables for a faster computation. The list of available processes and models that are available in the public version 10.2 is the following (the kinetic energy range for each type of interaction is given in parentheses):

Electrons:

- Elastic scattering (7.4 eV–1 MeV)
  - screened Rutherford and Brenner-Zaider formula below 200 eV [42]
  - updated alternative version by Uehara et al. [43]
  - partial wave framework model by Champion et al. [37]
- Ionization (10 eV–1 MeV)
  - dielectric formalism and first Born approximation using the Heller optical data [44] up to 1 MeV and low-energy corrections, derived from the work of Emfietzoglou [45]
  - improved alternative version by Emfietzoglou and Kyriakou [40]

- Electronic excitation (8 eV–1 MeV)
  - dielectric formalism and first Born approximation using the Heller optical data [44] and semi-empirical low-energy corrections derived from the work of Emfietzoglou [45]
  - improved alternative version by Emfietzoglou and Kyriakou [40]
- Vibrational excitation (2–100 eV)
  - cross section measurements in amorphous ice by Michaud et al. [46]
  - a factor of 2 is included to account for phase effects
- Dissociative attachment (4–13 eV)
  - cross section measurements by Melton [47]

Protons and hydrogen atoms:

- Electronic excitation (10 eV–100 MeV)
  - Miller and Green [48] speed scaling of e^- excitation at low energies, and Born and Bethe theories above 500 keV, from Dingfelder et al. [49]
- Ionization (100 eV–100 MeV)
  - Rudd semi-empirical approach [50] by Dingfelder et al. [49], and Born and Bethe theories and dielectric formalism above 500 keV (relativistic + Fermi density)
- Charge transfer (100 eV–100 MeV)
  - analytical parameterizations by Dingfelder et al. [49]

He^0, He^+, He^{2+}:

- Electronic excitation and ionization (1 keV–400 MeV)
  - speed and effective charge scaling from protons by Dingfelder et al. [51]
- Charge transfer (1 keV–400 MeV)
  - semi-empirical models from Dingfelder et al. [49, 52]

Li, Be, B, C, N, O, Si, and Fe ions:

- Ionization (0.5 MeV/u–1 TeV/u)
  - speed scaling and global effective charge by Booth and Grant [53]

As follows from this list, Geant4-DNA is capable of simulating protons with the kinetic energy of up to 100 MeV. Although this energy covers almost the full range of proton therapy accelerators, it does not cover the highest accelerator energies, which need to be as high as 230 MeV in order to treat deeply-seated tumors in the human body.

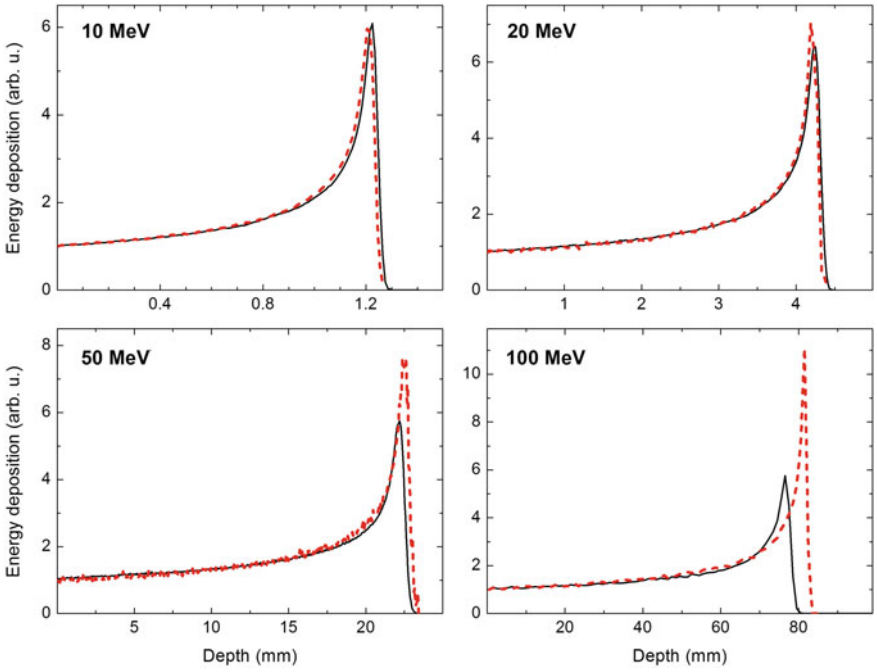

Fig. 1 Energy deposited in water medium along the path of 10, 20, 50, and 100 MeV protons. *Dashed curves* show the simulations performed by means Geant4-DNA physics, while *solid curves* shown the results obtained with binary cascade and standard electromagnetic physics

Figure 1 presents the distribution of dose calculated with the Geant4-DNA package (dashed curve) compared to that obtained with the standard physics plus binary cascade list (solid curve) for energies ranging from 10 to 100 MeV. In the case of a 10 MeV proton, the energy depositions obtained within the two approaches almost coincide with one another but the relative discrepancy in the position of the Bragg peak increases with increasing the projectile's energy. Although Geant4-DNA in some cases does not allow for an accurate quantitative description of the Bragg peak, this package is capable of determining the number of ionizations induced by protons as well as the electronic processes that may cause DNA damage. To illustrate this, we have simulated 1000 tracks of 10 MeV protons in liquid water. Table 1 shows the number of interactions of each kind which are produced by a single projectile. The distribution of these interactions along the proton's track for the three types of particles, namely, protons, hydrogen atoms, and electrons, is presented in Fig. 2. The Geant4-DNA simulations of the proton slow-down account for the ionization, excitation, and charge transfer interactions involving the projectile. However, they do not account for elastic scattering of the projectile from molecules of the medium. Thus, a projectile traversing the medium follows a straight line and the analysis of the total track does not give any additional information. As it will be discussed further

Table 1 Number of interactions of each type resulting from the propagation of a 10 MeV proton in water

Process name	No. of interactions
proton_G4DNAExcitation	68297.2
protons_G4DNAChargeDecrease	5315.6
hydrogen_G4DNAIonisation	6997.4
hydrogen_G4DNAExcitation	1117
hydrogen_G4DNAChargeIncrease	5312.25
e-_G4DNAElastic	1.18×10^8
e-_G4DNAIonisation	1.75×10^6
e-_G4DNAExcitation	296555
e-_G4DNAVibExcitation	1.33×10^7
e-_G4DNAAttachment	42529.9

in this chapter, elastic interactions play a significant role during the propagation of heavy particles in the medium, especially at the low kinetic energy, and this effect should be taken into consideration for a more accurate and complete picture. We note that the contribution of elastic scattering was included into the Geant4-DNA package very recently [41].

3 Extension of the Low-Energy Particle Simulation (LEPTS) Code

A general limitation of the most existing Monte Carlo track structure codes is that they do not describe very accurately the interaction of low-energy particles with molecular constituents of a medium [17]. Some codes actually stop modeling primary and secondary particles if their energies drop below 50–100 eV [54]. By means of the LEPTS code (see the review paper [5] and references therein), it has become possible to model dynamics of secondary species down to the (sub-)electronvolt scale. This Monte Carlo-based tool has been developed to address the molecular level mechanisms of biological damage and to describe radiation effects in nanovolumes in terms of induced molecular dissociations [6].

Recently, the LEPTS methodology has been extended to simulate explicitly the slowing-down of heavy charged particles propagating through a biological medium, accounting for the production of secondary particles, including low-energy electrons, and different molecular processes induced. As the first step, the attention has been focused on the simulation of intermediate- and low-energy protons traversing liquid water. In order to include protons into the simulation scheme, a comprehensive data set of integral and differential cross sections of elastic and inelastic scattering of protons from water molecules has been compiled. For that, experimental and

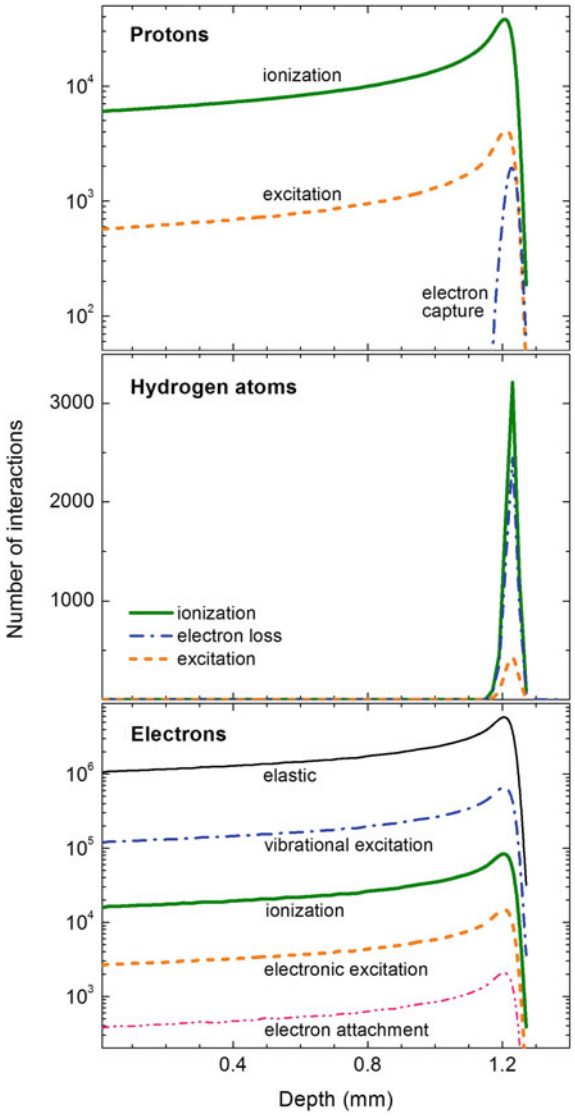

Fig. 2 Number of interactions of each type as a function of depth (in μm) for proton—(*upper panel*), neutral hydrogen—(*middle panel*) and electron—(*lower panel*) induced processes in water after the traverse of 1000 protons of 10 MeV energy

theoretical cross sections available in the literature have been carefully examined and verified. Development of a new database that includes adequate data for biologically relevant materials provides an opportunity for a more realistic, physically meaningful description of radiation damage in living tissue. Hence, the utilized approach allows one to study radiation effects on the nanoscale in terms of the number and the type of induced molecular processes. The next section provides an overview of the compiled data set used for the simulations performed with LEPTS.

3.1 Interaction Processes and Input Data

Generally, a track structure simulation of the charged particle propagation in a biological medium comprises a series of sampling steps that determine the distance between two successive interactions, as well as the type of interaction occurring at the selected point in space. These steps are routinely repeated for all primary and secondary particles until their kinetic energy becomes smaller than a pre-defined cutoff value. The interaction type is randomly selected according to the relative magnitude of the total cross section of all the processes. For the projectile-medium interaction, they are (i) ionization, capture, and excitation induced by a proton, and (ii) ionization, capture, excitation and electron loss induced by a hydrogen atom. The kinematics of the interaction is derived from single- and double-differential cross sections of the corresponding process. Secondary electrons are generated as a result of the ionization event; their energy is defined as the energy lost by the projectile minus the ionization potential of a target molecule. The formation and further evolution of all secondary species is simulated in full according to an explicit database of electron-induced molecular-level interactions. Up to now, the following processes involving electrons have been included in LEPTS: elastic scattering, ionization, electronic, vibrational and rotational excitations, dissociative electron attachment, and neutral dissociation (see Refs. [5, 17] and references therein).

One should note that several computer codes for proton transport in water have been reported in the literature so far (e.g., Refs. [7–9]). One of the most recently developed tools is the code called TILDA-V [11], which is based on quantum-mechanically calculated multiple differential and total cross sections for describing inelastic processes occurring during the slowing-down of protons in water and DNA. The advantage of the procedure implemented in LEPTS comes from much lower cutoff values for heavy charged projectiles and secondary electrons. In other words, all the particles are explicitly tracked in the simulation until they reach smaller energies. This allows one to get a more consistent picture of the radiation-induced processes occurring on the nanoscale. As noted above, this issue is crucial because low-energy secondary electrons, having the kinetic energy smaller than ionization or even excitation threshold of a water molecule, can produce significant biodamage as a result of dissociative electron attachment. In the TILDA-V code [11], the cutoff energy for protons and neutral hydrogen atoms is fixed to 10 keV, while the cutoff for secondary electrons corresponds to the electronic excitation threshold of a water molecule, that is 7.4 eV. In the simulation performed with LEPTS, the heavy projectiles are tracked down to approximately 1 eV as follows from the data set described below, and the electrons can be tracked until their final thermalization at the sub-eV scale [5, 16].

3.1.1 Integral Cross Sections

Integral cross sections for elastic and inelastic interactions of 1 eV–1 MeV protons with water molecules are summarized in Fig. 3. Ionization, excitation, and charge

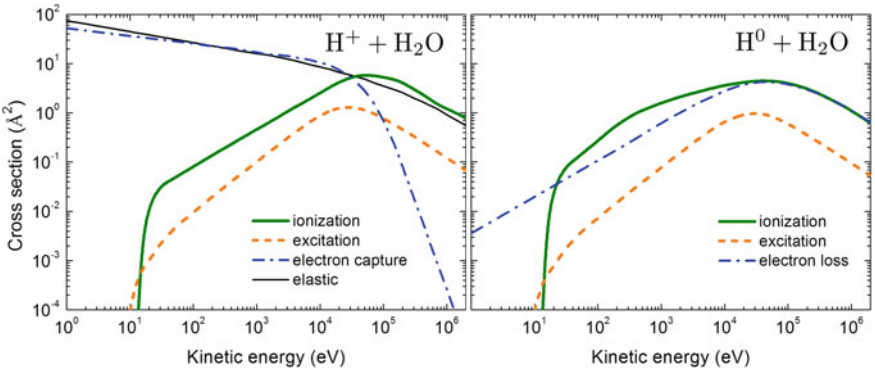

Fig. 3 Integral cross sections for collision of protons and neutral hydrogen atoms with water molecules that have been used as an input for the simulations. Details on data sources are provided in the text

transfer (electron capture) were considered as inelastic processes for H^+ projectiles (left panel). As a result of the charge transfer process, an electron from a water molecule is transferred to the moving slow proton to form a neutral hydrogen atom; the corresponding inelastic cross sections for the neutral projectile are shown in the right panel. We have included the processes of ionization and excitation of a water molecule by H^0 and also accounted for a probability of electron loss (stripping) by the neutral atom.

The ionization cross section by protons has been produced as a result of a thorough analysis of experimental and theoretical data, including recent measurements of the production of different charged fragments [55, 56], and the corresponding classical, semi-classical and *ab initio* calculations [57–59]. The excitation and charge transfer (both electron capture and loss) cross sections for both charged and neutral projectiles were taken from Refs. [11, 49] which are based on a semi-empirical model by Green et al. [48, 60]. As indicated in Ref. [49], parameters of the model were chosen to fit the calculated excitation cross sections to those obtained within the first Born approximation at higher projectile energies. We also accounted for elastic scattering of protons from water molecules (nuclear scattering) which becomes important at lower incident energies of about and below 10 keV. Integral elastic cross section data were taken from Refs. [41, 61].

3.1.2 Total Ionization Cross Section

Data on the total ionization cross section, which have been used in the simulations, are presented in Fig. 4. The data set includes the cross section taken from ICRU Report 49, as well as results of experimental measurements. Older experiments done by Rudd and co-workers [62, 63] were focused mainly on determining the total electron production cross section by the integration of their doubly differential electron

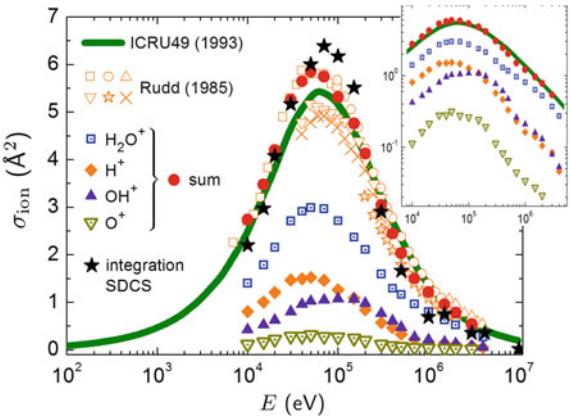

Fig. 4 Total ionization cross sections for collision of protons with water molecules that have been used as an input for the simulations. *All symbols* except for *filled stars* indicate experimental data from Ref. [62] and interpolated experimental data from Refs. [55, 56, 64] on the production of charged fragments. *Filled stars* correspond to the integrated values of single-differential cross sections described in Sect. 3.1.3

emission cross sections. More recent experiments [55, 56, 64] allowed one to get the information on production of different charged fragments, namely H_2O^+, H^+, OH^+, and O^+. In the compiled data set, we have used these data accompanying with the results of recent theoretical studies [57–59]. In order to get smooth cross sections (shown in Fig. 4 by symbols), we did spline interpolation of the experimental data from different measurements [55, 56, 64]. The figure illustrates that the results from the ICRU Report (solid curve) almost coincide with the recent experimental data (filled circles) at the energies about 10–20 keV and above 1 MeV. In the Bragg peak region, at about 50–100 keV, the new data exceed the already established ones by about 10 %. In the compiled data set, we used the new experimental data as a more preferred source. Thus, the resulting curve (shown by a thick solid line in Fig. 3) comprises the experimental data [55, 56, 64] in the range 10 keV–1 MeV and the data from the ICRU 49 Report at lower energies. Note that thus compiled data set is consistent, within the 10 % accuracy, with the integrated single-differential cross sections (filled stars in Fig. 4), described below.

3.1.3 Differential Ionization Cross Sections

Double-differential cross sections (in terms of the kinetic energy and angular distribution of secondary electrons) for 1.5-, 1.0-, 0.5-, 0.3-, 0.1-MeV, and for 15-keV protons were taken from the experimental data of Toburen and Wilson [65], Bolorizadeh and Rudd [63], and the calculations of Senger and Rechenmann [66]. The cited papers

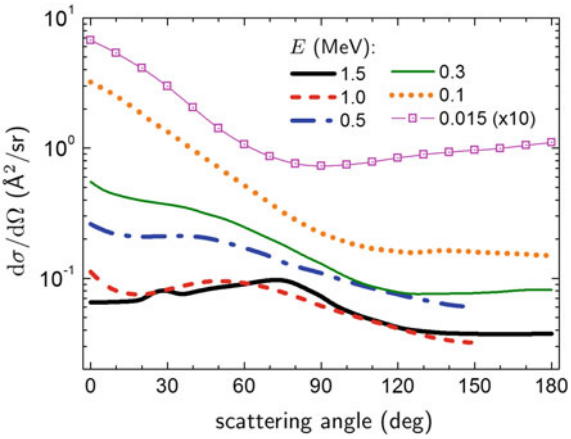

Fig. 5 Single-differential cross section $\mathrm{d}\sigma/\mathrm{d}\Omega$ describing angular distribution of secondary electrons ejected from a water molecule after the collision with protons. See the text for the details on data sources

presented the data for secondary electrons with kinetic energy ε from about 10 eV up to 2.2 keV. These data were interpolated, and the compiled dependencies were integrated over the kinetic energy of emitted electrons to get their angular distribution. Thus calculated single-differential (in terms of electron emission angle) cross sections, $\mathrm{d}\sigma/\mathrm{d}\Omega$, are shown in Fig. 5.

Single-differential (in terms of kinetic energy of secondary electrons) cross sections, $\mathrm{d}\sigma/\mathrm{d}\varepsilon$, were compiled based on the experimental data from Refs. [63, 67] and supplemented with the calculations from Refs. [9, 49, 68]. A thorough compilation of the data from different sources has allowed us to produce an explicit set of cross sections for 10-, 4.2-, 3.0-, 1.5-, 1.0-, 0.5-, 0.3-, 0.1-MeV and 70-, 50-, 30-, 20-, 15-, and 10-keV protons (see Figs. 6 and 7).

3.1.4 Self-consistency of the Data Set

An important issue of a database created from different experimental and theoretical sources is reliability of the input data. To elaborate on this issue, we have performed several self-consistency checks, namely we compared the integrated double-differential cross sections, $\int \frac{\mathrm{d}^2\sigma}{\mathrm{d}\Omega\,\mathrm{d}\varepsilon}\mathrm{d}\Omega$, with the single-differential cross section, $\mathrm{d}\sigma/\mathrm{d}\varepsilon$, taken from separate sources (see Fig. 7) and then also compared the integrated energy spectra $\int \frac{\mathrm{d}\sigma}{\mathrm{d}\varepsilon}\mathrm{d}\varepsilon$ with the total ionization cross section σ_{ion} (see Fig. 4). The agreement between the differential cross sections is very good, while the relative discrepancy between the integrated $\mathrm{d}\sigma/\mathrm{d}\varepsilon$ and σ_{ion} does not exceed 10 % confirming the reasonable level of accuracy of the input data for simulations.

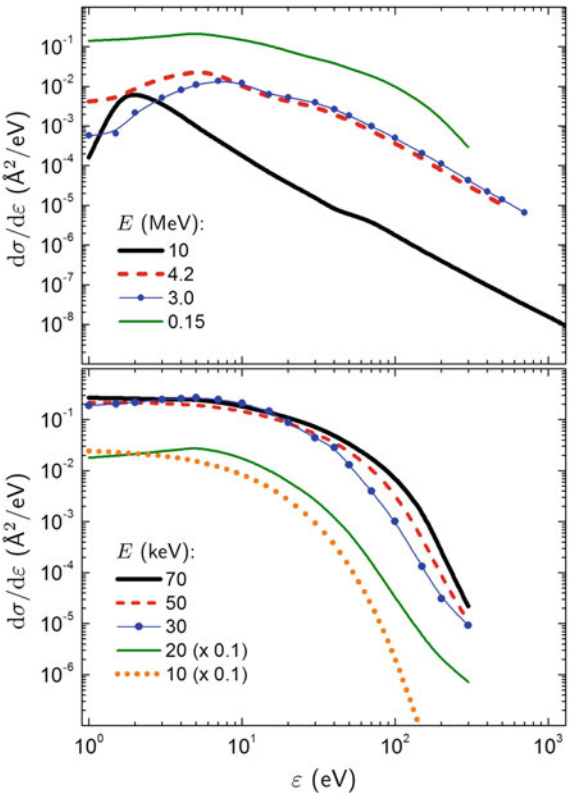

Fig. 6 Energy spectra of secondary electrons, $d\sigma/d\varepsilon$, emitted after irradiation with 10 MeV–10 keV protons. The data set is compiled from [63, 67] and theoretical calculations [9, 49, 68]

4 Results of the Simulations

As a case study, we present the results of the simulation of the slowing-down of 1 MeV protons in liquid water (1 g/cm^3 density) until their final thermalization at the few-eV scale. Charged heavy particles of such energies contribute greatly to the maximum of energy deposition in the Bragg peak region [20]. Hence, it is of significant interest to analyze the type and the number of molecular dissociations in the medium. In this study, we have simulated one million tracks to get good statistics. As noted above, data for single water molecules in the gas phase were used as input parameters but the tracks of all primary and secondary particles were modeled in the liquid phase by considering the liquid density and correcting the cross section values in order to introduce screening effects from the surrounding molecules [5]. Figure 8 illustrates the number of interactions as a function of the depth (in μm) for different scattering processes, including elastic collisions and different types of inelastic events. The maximum penetration of 1 MeV protons in water is about 25 μm, and the position of the Bragg peak corresponds to the kinetic energy of about 100 keV. The simulations performed by means of LEPTS provide a more detailed

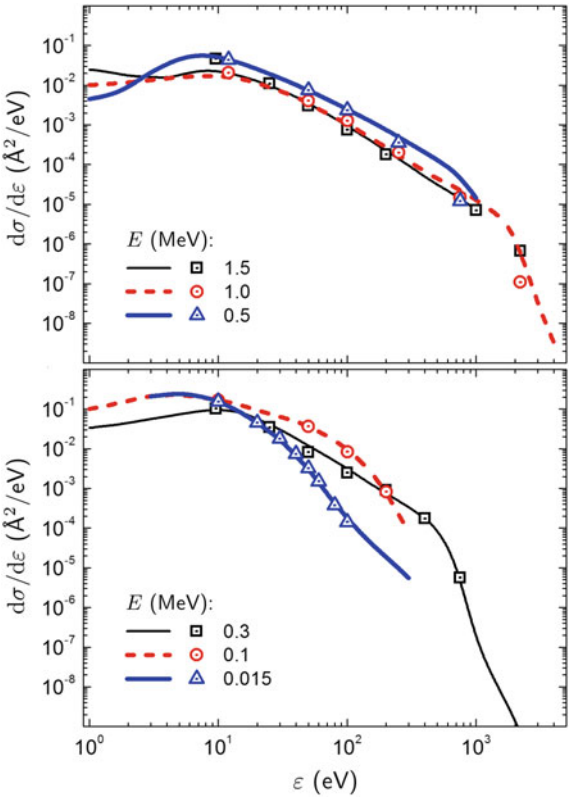

Fig. 7 Same as Fig. 6 but for different projectile energies (*solid* and *dashed curves*). *Symbols* correspond to the integrated values of double-differential cross sections compiled from Refs. [63, 65, 66]

description of different processes occurring on the nanoscale, as compared to the simulations performed with Geant4-DNA (see Fig. 2). As noted above, the LEPTS model explicitly accounts for elastic scattering of neutral and charged projectiles, which provides a substantial contribution to the total number of interaction events. Figure 8 demonstrates that all the interactions associated with protons and electrons stop at the depth of about 23 μm, while elastic collisions between neutral hydrogen atoms and the water molecules also contribute at further penetration distances up to 25 μm. Therefore, a detailed description of molecular dissociations induced by low-energy hydrogen atoms colliding with biologically relevant molecules is of significant importance. This information can be obtained, for instance, from advanced *ab initio* calculations.

The analysis of the interactions presented in Fig. 8 allows for a detailed evaluation of the energy deposition as a function of the penetration depth in the medium. This dependence is shown in Fig. 9. The figure illustrates that the dominating contribution to the energy deposition is related to the elastic and inelastic processes induced by secondary electrons which is a typical feature of irradiation with protons and heavier ions. The energy deposited by electrons has an interesting feature that results

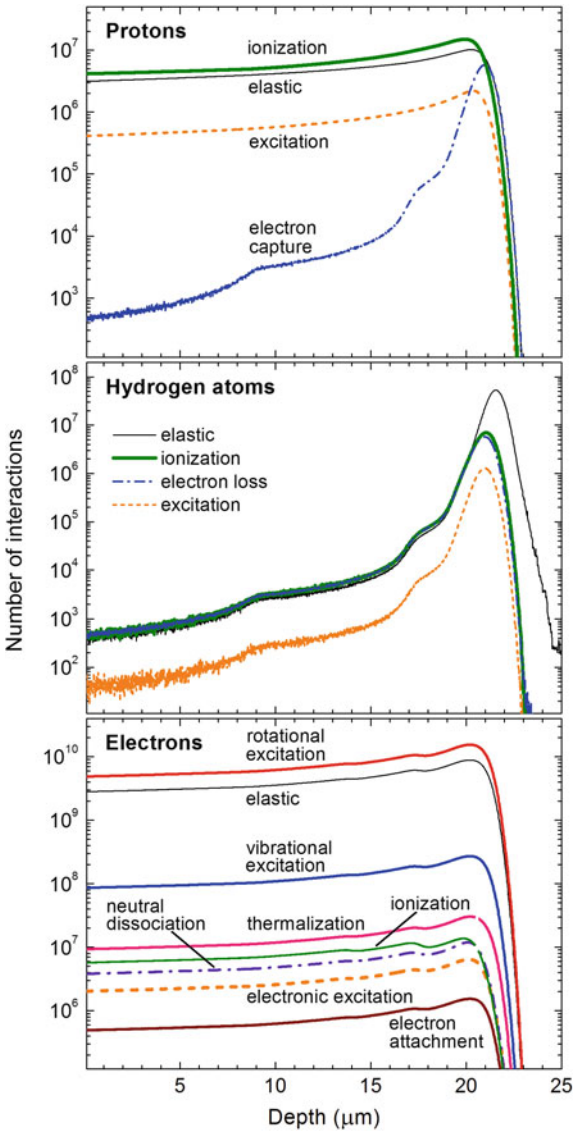

Fig. 8 Number of interactions of each type as a function of depth (in μm) for proton—(*upper panel*), neutral hydrogen—(*middle panel*) and electron—(*lower panel*) induced processes in water after the traverse of 10^6 protons of 1 MeV initial energy, as simulated by means of LEPTS

in a bump in the range between approximately 14 and 18 μm. This feature may be associated with an increased number of secondary electrons produced at these distances by the projectiles. As demonstrated in Fig. 8, this range of penetration corresponds to a gradual increase in the number of elastic and inelastic processes involving neutral hydrogen atoms. The electrons produced as a result of ionization of H atoms deposit their energy within several microns until they slow down to the energies below the ionization potential of a water molecule. This results in a small

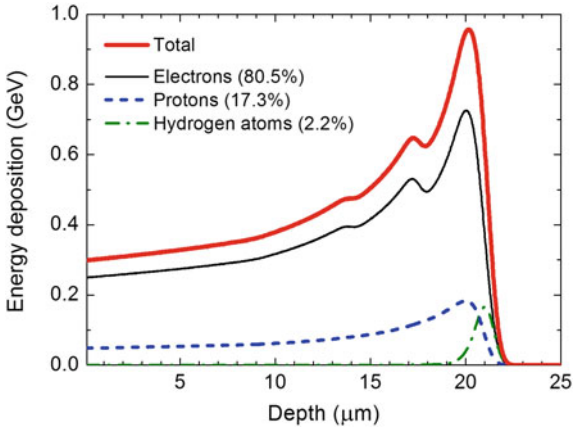

Fig. 9 Energy deposition of 10^6 incident protons of 1 MeV energy each in liquid water as a function of depth

dip at about 18 μm observed in the number of electron-induced ionizations (see the lower panel of Fig. 8). One should note also that the maximal energy deposition by electrons and protons corresponds to the position of the Bragg peak, while the energy deposited by neutral hydrogen atoms, although representing a minor contribution, is localized at further penetration depth beyond the maximum of the Bragg peak. This feature additionally underlines the importance of the accurate description of interactions induced by the neutral projectiles with very low kinetic energy.

Acknowledgements We acknowledge the financial support received from the European Union Seventh Framework Programme (PEOPLE-2013-ITN-ARGENT project) under grant agreement no. 608163 and from the Spanish Ministerio de Economia y Competitividad (Project no. FIS2012-31230).

References

1. Garcia Gomez-Tejedor G, Fuss MC (eds) (2012) Radiation damage in biomolecular systems. Springer Science+Business Media B.V
2. Boudaïffa B, Cloutier P, Hunting D, Huels MA, Sanche L (2000) Resonant formation of DNA strand breaks by low-energy (3 to 20 eV) electrons. Science 287:1658–1660
3. Surdutovich E, Solov'yov AV (2014) Multiscale approach to the physics of radiation damage with ions. Eur Phys J D 68:353
4. Oller JC, Ellis-Gibbings L, Ferreira da Silva F, Limão-Vieira P, García G (2015) Novel experimental setup for time-of-flight mass spectrometry ion detection in collisions of anionic species with neutral gas-phase molecular targets. EPJ Tech Instrum 2:13
5. Blanco F, Muñoz A, Almeida D, Ferreira da Silva F, Limão-Vieira P, Fuss MC, Sanz AG, García G (2013) Modelling low energy electron and positron tracks in biologically relevant media. Eur Phys J D 67:199
6. Muñoz A, Pérez JM, García G, Blanco F (2005) An approach to Monte Carlo simulation of low-energy electron and photon interactions in air. Nucl Instrum Meth A 536:176–188
7. Krämer M, Kraft G (1994) Calculations of heavy-ion track structure. Radiat Environ Biophys 33:91–109

8. Friedland W, Jacob P, Bernhardt P, Paretzke HG, Dingfelder M (2003) Simulation of DNA damage after proton irradiation. Radiat Res 159:401–410
9. Nikjoo H, Uehara S, Emfietzoglou D, Cucinotta FA (2006) Track-structure codes in radiation research. Radiat Meas 41:1052–1074
10. Incerti S et al (2010) Comparison of GEANT4 very low energy cross section models with experimental data in water. Med Phys 37:4692–4708
11. Quinto MA et al (2015) Proton track structure code in biological matter. J Phys: Conf Ser 583:012049
12. Huels MA, Boudaïffa B, Cloutier P, Hunting D, Sanche L (2003) Single, double, and multiple double strand breaks induced in DNA by 3–100 eV electrons. J Am Chem Soc 125:4467–4477
13. Pan X, Cloutier P, Hunting D, Sanche L (2003) Dissociative electron attachment to DNA. Phys Rev Lett 90:208102
14. Baccarelli I, Gianturco FA, Scifoni E, Solov'yov AV, Surdutovich E (2010) Molecular level assessments of radiation biodamage. Eur Phys J D 60:1–10
15. FP7 Initial Training Network Project "Advanced Radiotherapy, Generated by Exploiting Nanoprocesses and Technologies" (ARGENT). http://www.itn-argent.eu
16. Arce P, Muñoz A, Moraleda M, Ros JMG, Blanco F, Perez JM, García G (2015) Integration of the low-energy particle track simulation code in Geant4. Eur Phys J D 69:188
17. Fuss MC, Ellis-Gibbings L, Jones DB, Brunger MJ, Blanco F, Muñoz A, Limão-Vieira P, García G (2015) The role of pyrimidine and water as underlying molecular constituents for describing radiation damage in living tissue: a comparative study. J Appl Phys 117:214701
18. Agostinelli S et al (2003) Geant4—a simulation toolkit. Nucl Instr Meth A 506:250–303
19. Allison J et al (2006) Geant4 developments and applications. IEEE Trans Nucl Sci 53:270–278
20. Schardt D, Elsässer T, Schulz-Ertner D (2010) Heavy-ion tumor therapy: physical and radiobiological benefits. Rev Mod Phys 82:383–425
21. Paganetti H, Jiang H, Parodi K, Slopsema R, Engelsman M (2008) Clinical implementation of full Monte Carlo dose calculation in proton beam therapy. Phys Med Biol 53:4825–4853
22. Petti PL (1996) Evaluation of a pencil-beam dose calculation technique for charged particle radiotherapy. Int J Radiat Oncol Biol Phys 35:1049–1057
23. Schaffner B, Pedroni E, Lomax A (1999) Dose calculation models for proton treatment planning using a dynamic beam delivery system: an attempt to include density heterogeneity effects in the analytical dose calculation. Phys Med Biol 44:27–41
24. Soukup M, Alber M (2007) Influence of dose engine accuracy on the optimum dose distribution in intensity-modulated proton therapy treatment plans. Phys Med Biol 52:725–740
25. Soukup M, Fippel M, Alber M (2005) A pencil beam algorithm for intensity modulated proton therapy derived from Monte Carlo simulations. Phys Med Biol 50:5089–5104
26. Szymanowski H, Oelfke U (2002) Two-dimensional pencil beam scaling: an improved proton dose algorithm for heterogeneous media. Phys Med Biol 47:3313–3330
27. Tourovsky A, Lomax AJ, Schneider U, Pedroni E (2005) Monte Carlo dose calculations for spot scanned proton therapy. Phys Med Biol 50:971–981
28. Titt U et al (2008) Assessment of the accuracy of an MCNPX-based Monte Carlo simulation model for predicting three-dimensional absorbed dose distributions. Phys Med Biol 53:4455–4470
29. Paganetti H (2012) Range uncertainties in proton therapy and the role of Monte Carlo simulations. Phys Med Biol 57:R99–R117
30. Pia MG, Begalli M, Lechner A, Quintieri L, Saracco P (2010) Physics-related epistemic uncertainties in proton depth dose simulation. IEEE Trans Nucl Sci 57:2805–2830
31. Lewis HW (1950) Multiple scattering in an infinite medium. Phys Rev 78:526–529
32. Moteabbed M, España S, Paganetti H (2011) Monte Carlo patient study on the comparison of prompt gamma and PET imaging for range verification in proton therapy. Phys Med Biol 56:1063–1082
33. Robert C et al (2013) Distributions of secondary particles in proton and carbon-ion therapy: a comparison between GATE/Geant4 and FLUKA Monte Carlo codes. Phys Med Biol 58:2879–2899

34. Jarlskog CZ, Paganetti H (2008) Physics settings for using the Geant4 toolkit in proton therapy. IEEE Trans Nucl Sci 55:1018–1025
35. Chauvie S, Francis Z, Guatelli S, Incerti S, Mascialino B, Moretto P, Nieminen P, Pia MG (2007) Geant4 physics processes for microdosimetry simulation: design foundation and implementation of the first set of models. IEEE Trans Nucl Sci 54:2619–2628
36. Francis Z, Incerti S, Capra R, Mascialino B, Montarou G, Stepan V, Villagrasa C (2011) Molecular scale track structure simulations in liquid water using the Geant4-DNA Monte-Carlo processes. Appl Radiat Isot 69:220–226
37. Champion C, Incerti S, Aouchiche H, Oubaziz D (2009) A free-parameter theoretical model for describing the electron elastic scattering in water in the Geant4 toolkit. Radiat Phys Chem 78:745–750
38. Champion C, Incerti S, Tran HN, El Bitar Z (2012) Electron and proton elastic scattering in water vapour. Nucl Instrum Meth B 273:98–101
39. Champion C et al (2013) Proton transport in water and DNA components: a Geant4 Monte Carlo simulation. Nucl Instrum Meth B 306:165–168
40. Kyriakou I, Incerti S, Francis Z (2015) Improvements in Geant4 energy-loss model and the effect on low-energy electron transport in liquid water. Med Phys 42:3870–3876
41. Tran HN et al (2015) Modeling proton and alpha elastic scattering in liquid water in Geant4-DNA. Nucl Instrum Meth B 343:132–137
42. Brenner DJ, Zaider M (1984) A computationally convenient parameterisation of experimental angular distributions of low energy electrons elastically scattered off water vapour. Phys Med Biol 29:443–447
43. Uehara S, Nikjoo H, Goodhead DT (1993) Cross-sections for water vapour for the Monte Carlo electron track structure code from 10 eV to the MeV region. Phys Med Biol 38:1841–1858
44. Heller JM Jr, Hamm RN, Birkhoff RD, Painter LR (1974) Collective oscillation in liquid water. J Chem Phys 60:3483–3486
45. Emfietzoglou D (2003) Inelastic cross-sections for electron transport in liquid water: a comparison of dielectric models. Radiat Phys Chem 66:373–385
46. Michaud M, Wen A, Sanche L (2003) Cross sections for low-energy ($1 - 100$ eV) electron elastic and inelastic scattering in amorphous ice. Radiat Res 159:3–22
47. Melton CE (1972) Cross sections and interpretation of dissociative attachment reactions producing OH^-, O^-, and H^- in H_2O. J Chem Phys 57:4218–4225
48. Miller JH, Green AES (1973) Proton energy degradation in water vapor. Radiat Res 54:343–363
49. Dingfelder M, Inokuti M, Paretzke HG (2000) Inelastic-collision cross sections of liquid water for interactions of energetic protons. Radiat Phys Chem 59:255–275
50. Rudd ME, Kim Y-K, Madison DH, Gay TJ (1992) Electron production in proton collisions with atoms and molecules: energy distributions. Rev Mod Phys 64:441–490
51. Dingfelder M, Jorjishvili IG, Gersh JA, Toburen LH (2006) Heavy ion track structure simulations in liquid water at relativistic energies. Radiat Prot Dos 122:26–27
52. Dingfelder M, Toburen LH, Paretzke HG (2005) An effective charge scaling model for ionization of partially dressed helium ions with liquid water. In: Proceedings of the Monte Carlo 2005 Topical Meeting, Chattanooga, TN, 17–21 April 2005, American Nuclear Society, La Grange Park, IL, pp 1–12
53. Booth W, Grant IS (1965) The energy loss of oxygen and chlorine ions in solids. Nucl Phys 63:481–495
54. Muñoz A, Blanco F, Oller JC, Pérez JM, García G (2007) Advances in quantum chemistry. In: Sabin JR, Brändas E (eds). vol 52, pp 21–57. Academic Press
55. Gobet F et al (2004) Ionization of water by $(20 - 150)$-keV protons: separation of direct-ionization and electron-capture processes. Phys Rev A 70:062716
56. Luna H et al (2007) Water-molecule dissociation by proton and hydrogen impact. Phys Rev A 75:042711
57. Errea LF, Illescas C, Méndez L, Pons B, Rabadán I, Riera A (2007) Classical calculation of ionization and electron-capture total cross sections in $H^+ + H_2O$ collisions. Phys Rev A 76:040701(R)

58. Murakami M, Kirchner T, Horbatsch M, Lüdde HJ (2012) Single and multiple electron removal processes in proton-water-molecule collisions. Phys Rev A 85:052704
59. Errea LF, Illescas C, Méndez L, Rabadán I (2013) Ionization of water molecules by proton impact: two nonperturbative studies of the electron-emission spectra. Phys Rev A 87:032709
60. Green AES, McNeal RJ (1971) Analytic cross sections for inelastic collisions of protons and hydrogen atoms with atomic and molecular gases. J Geophys Res 76:133–144
61. Uehara S, Toburen LH, Nikjoo H (2001) Development of a Monte Carlo track structure code for low-energy protons in water. Int J Radiat Biol 2:139–154
62. Rudd ME, Goffe TV, DuBois RD, Toburen LH (1985) Cross sections for ionization of water vapor by 7–4000-keV protons. Phys Rev A 31:492–494
63. Bolorizadeh MA, Rudd ME (1986) Angular and energy dependence of cross sections for ejection of electrons from water vapor. II. 15–150-keV proton impact. Phys Rev A 33:888–892
64. Werner U, Beckord K, Becker J, Lutz HO (1995) 3D imaging of the collision-induced Coulomb fragmentation of water molecules. Phys Rev Lett 74:1962–1965
65. Toburen LH, Wilson WE (1977) Energy and angular distributions of electrons ejected from water vapor by 0.3–1.5 MeV protons. J Chem Phys 66:5202–5213
66. Senger B, Rechenmann RV (1984) Angular and energy distributions of δ-rays ejected from low-Z molecular targets by incident protons and α particles. Nucl Instrum Meth B 2:204–207
67. Wilson WE, Miller JH, Toburen LH, Manson ST (1984) Differential cross sections for ionization of methane, ammonia, and water vapor by high velocity ions. J Chem Phys 80:5631–5638
68. de Vera P, Garcia-Molina R, Abril I, Solov'yov AV (2013) Semiempirical model for the ion impact ionization of complex biological media. Phys Rev Lett 110:148104